

A Method for Detecting Spatio-temporal Correlation Anomalies of WSN Nodes Based on Topological Information Enhancement and Time-frequency Feature Extraction

Miao Ye, Ziheng Wang, Yong Wang and Junqi Chen

Abstract—Existing anomaly detection methods for Wireless Sensor Networks (WSNs) generally suffer from insufficient extraction of spatio-temporal correlation features, reliance on either time-domain or frequency-domain information alone, and high computational overhead. To address these limitations, this paper proposes a topology-enhanced spatio-temporal feature fusion anomaly detection method, TE-MSTAD. First, building upon the RWKV model with linear attention mechanisms, a Cross-modal Feature Extraction (CFE) module is introduced to fully extract spatial correlation features among multiple nodes while reducing computational resource consumption. Second, a strategy is designed to construct an adjacency matrix by jointly learning spatial correlation from time-frequency domain features. Different graph neural networks are integrated to enhance spatial correlation feature extraction, thereby fully capturing spatial relationships among multiple nodes. Finally, a dual-branch network TE-MSTAD is designed for time-frequency domain feature fusion, overcoming the limitations of relying solely on the time or frequency domain to improve WSN anomaly detection performance. Testing on both public and real-world datasets demonstrates that the TE-MSTAD model achieves F1 scores of 92.52% and 93.28%, respectively, exhibiting superior detection performance and generalization capabilities compared to existing methods.

Index Terms—Wireless sensor networks, anomaly detection, time-frequency domain fusion, graph neural networks, information enhancement.

I. INTRODUCTION

WIRELESS SENSORS networks (WSNs) are self-organizing networks composed of numerous distributed sensor nodes, typically employing multi-hop routing for data transmission. WSN nodes can sense and transmit environmental physical data such as temperature, humidity, carbon dioxide concentration, and light intensity. Due to their convenient deployment and flexible network topology, WSNs are widely applied in various fields including defense and military [1], industrial environmental monitoring [2], medical monitoring [3], smart agriculture [4], and smart city transportation [5].

However, WSN deployments frequently encounter external

interference from complex natural environments or mutual interference between indoor nodes [6]. Furthermore, WSN nodes themselves face limitations from internal factors such as insufficient power supply, software programming defects, long-term hardware aging, and unstable signal transmission/reception [7], leading to data collection and transmission distortion and anomalies. Designing efficient and practical WSN anomaly node detection algorithms is crucial for ensuring stable operation and reliable application of WSNs[8].

Typically, data collected individually for a single physical quantity can be regarded as a single-time-series data point [9]. Data collected simultaneously for multiple physical quantities is considered multiple time-series data, referred to as multimodal time-series data [10]. Such multi-time-series data may consist of different physical quantities collected from the same node or physical quantities collected separately from different nodes. Anomalies in single-time-series data from WSNs encompass three types of temporal correlations: point anomalies, context anomalies, and collective anomalies [11]. A point anomaly occurs when data at a specific time point significantly deviates from the normal data at other time points within that time series. A context anomaly arises when, within the specific contextual scenario of that time series, some data points diverge from the majority of normal data points. Context anomalies are localized and context-dependent; they may be considered normal in other contextual scenarios. Collective anomalies occur when individual data points may not be anomalous on their own, but a group of data points collectively exhibits abnormal behavior. Within a single time series, collective anomalies typically manifest as repeated fluctuations across multiple consecutive data points. Anomalies in multi-temporal data within WSNs refer to spatio-temporal correlation anomalies among these time series. This arises because multimodal time series data collected by the same sensor node typically exhibit spatio-temporal correlations [9], and modal data collected by different sensor nodes also often display such correlations [11]. When a fire occurs in the environment, temperature data collected by sensors around the fire center should all increase, indicating spatial positive correlation between different time-series data collected by different nodes. When such temporal or spatial correlations in collected multi-

temporal data are disrupted, this phenomenon is termed a correlation anomaly [11].

Regarding the aforementioned spatio-temporal correlation anomalies in WSNs, researchers have progressively developed a series of anomaly detection methods for WSN correlations. These WSN anomaly detection approaches have evolved from traditional statistical methods to deep learning, driven by application requirements and technological advancements. Early anomaly detection methods included statistical-based approaches and traditional machine learning techniques, such as threshold detection [12] and clustering methods [2]. However, these approaches have shown limitations in handling applications featuring complex topological structures[13], high-dimensional multimodal features[14], and scenarios involving both long-term dependencies and spatiotemporal correlations [15]. With the rise of deep learning technologies, convolutional neural networks (CNN) [16], recurrent neural networks (RNN) [17], long short-term memory (LSTM) networks [18], and gated recurrent units (GRU) [19] have emerged. These methods can capture nonlinear relationships in data and automatically extract features using deep networks, thereby enhancing the ability to extract high-dimensional temporal features to some extent. Subsequently, the Transformer [20] enhanced global feature extraction and the capture of long-range dependencies. It mitigated gradient explosion and vanishing gradient issues when processing long-range dependent time series data, enabling better recognition of complex multivariate time series anomaly patterns and thus improving detection performance. It has now become a crucial tool in anomaly detection methods. Furthermore, to effectively mine complex spatial correlation features among nodes in WSNs, graph neural networks (GNN) [15] have been progressively integrated into the spatial feature extraction process for WSN-collected data. However, current mainstream deep learning-based WSN time-series anomaly detection methods, such as those based on Transformers and GNNs, still exhibit the following shortcomings:

First, existing WSN anomaly detection methods lack sufficient capability to extract spatio-temporal correlation features across multiple nodes and modalities. Current deep learning-based WSN anomaly detection approaches typically focus solely on detecting anomalies in correlations between different modalities within the same sensor node or within the same modality across different sensor nodes. They fail to address the detection of spatio-temporal correlation anomalies across different modalities and sensor nodes. Second, due to the quadratic growth of computational complexity with sequence length in self-attention mechanisms, Transformers incur significantly increased computational overhead and memory consumption when processing long sequences. This leads to prolonged training times and excessive resource consumption [21]. Furthermore, since WSN-collected data contains not only sensor node attribute features but also spatial topology information between nodes[13], existing GNN-based anomaly detection methods suffer from weak generalization capabilities. This is due to their monolithic model structures and lack of

effective topology information augmentation mechanisms, making it difficult to fully capture the complex spatial topology features in WSNs and thereby reducing anomaly detection performance. Finally, based on the uncertainty principle in time-series representation [22] demonstrates that data exhibits significant differences in temporal and frequency domains for different anomaly types. When a certain type of anomaly is difficult to detect in the time domain, detection performance in the frequency domain significantly improves, and vice versa [23]. However, most existing WSN anomaly detection methods perform feature analysis and extraction solely on signals in either the time domain or frequency domain, limiting the performance of WSN anomaly detection. For example, traditional time-domain analysis has limited capability in extracting periodic features from data, reducing detection performance for anomalies exhibiting periodic variations. In contrast, the frequency domain can reveal the periodic structure and energy distribution characteristics of signals, enabling more effective identification.

To address the aforementioned issues, this paper proposes a topology-enhanced multi-modal spatio-temporal anomaly detection (TE-MSTAD) method, the main contributions of this work are as follows:

1. To address the issue that existing methods are difficult to fully extract the temporal correlation features of multiple temporal modalities, this paper adds a designed CFE module to the RWKV model. While maintaining the parallel training of RWKV to handle long-distance dependent tasks and reducing the computational complexity, it can fully extract the temporal correlation features between different temporal modalities. It is suitable for anomaly detection in multi-temporal modal scenarios of WSN.

2. To address the issue that existing methods are difficult to fully extract the spatial correlation features of multiple nodes, this paper proposes two topological information enhancement strategies. Firstly, this paper proposes a method for calculating the similarity between nodes through time-domain and frequency-domain features, and builds a graph adjacency matrix containing time-frequency domain information. Secondly, this paper proposes a method for enhancing spatial feature extraction based on graph neural network ensemble. By constructing a series of different graph neural network complex models, the spatial features that different models focus on outputting are obtained. Therefore, this design can fully extract the spatial correlation features among multiple nodes and is suitable for anomaly detection in the multi-node scenario of WSN.

3. Aiming at the problem that the existing methods only rely on a single time domain or frequency domain for feature extraction, and the anomaly detection performance is limited due to the uncertainty principle of time series representation, this paper designs a dual-branch network TE-MSTAD based on feature extraction in the time and frequency domains. This network can combine information in the time domain and frequency domain for WSN anomaly detection, making up for the limitations of relying on a single time domain or frequency

domain, thereby improving the performance of WSN anomaly detection.

The remainder of this paper is structured as follows: Section II reviews relevant research progress in the field of WSN anomaly detection; Section III formally defines the research problem and briefly introduces the fundamental principles of the RWKV model; Section IV elaborates on the overall framework and constituent modules of the proposed TE-MSTAD model; Section V demonstrates the performance of the proposed method on publicly available indoor datasets and real-world outdoor datasets, along with comparative analysis against existing approaches; finally, Section VI summarizes the work and outlines future research directions.

II. RELATED WORK

In recent years, with the widespread application of WSNs, accurately and efficiently detecting anomalous data has become a key concern for both academia and industry. This section reviews existing studies, focusing on the development and evolution of WSN anomaly detection methods and frequency domain analysis approaches.

A. Deep-learning Model for Anomaly Detection in WSNs

Historically, WSN anomaly detection primarily relied on traditional statistical methods and machine learning-based approaches. Statistical methods include Kalman filtering, autoregressive integrated moving average (ARIMA) models, and principal component analysis (PCA), while machine learning-based methods encompass clustering-based anomaly detection and dimension reduction techniques. Ref. [12] proposed a novel online adaptive Kalman filtering method specifically for real-time anomaly detection in WSNs by dynamically adjusting filtering parameters and anomaly detection thresholds in response to real-time data. Ref. [2] proposes a monotonic split-and-conquer scheme for detecting anomalous sensor data by leveraging spatio-temporal correlations between neighboring sensors through principal component analysis. Furthermore, these methods often exhibit high computational complexity when handling complex, high-dimensional data, making them ill-suited for real-time detection demands on large-scale datasets [24].

In contrast, deep learning methods can automatically learn complex features and patterns in data, demonstrating greater adaptability and accuracy when handling high-dimensional, nonlinear data. Furthermore, deep learning approaches can capture long-term dependencies within data, making them highly suitable for WSN data with time-series characteristics. Ref. [25] proposes a data-driven anomaly detection method termed Median Filter-Stacked Long Short-Term Memory-Exponentially Weighted Moving Average for anomaly identification. Building upon the original RWKV model, ref. [21] proposes a novel detection scheme for harsh environments using an ensemble of autoencoders, Gaussian mixture models, and K-means, focusing on analyzing single-round forwarding rate time series of nodes. These methods demonstrate superior performance compared to traditional and machine learning

approaches when handling complex, high-dimensional, long-term sequence data. However, such approaches focus solely on the temporal correlation features of WSN time-series data, making it difficult to extract latent spatial correlation information from graph-structured WSN data. Consequently, they cannot achieve spatial correlation anomaly detection for WSN time-series data.

With the emergence of graph neural networks (GNNs), anomaly detection methods leveraging these models can aggregate node information via adjacency matrices, effectively extracting spatial correlation features between nodes. Ref. [26] proposes a collaborative approach where pattern mining guides GNN algorithms to aggregate local information through connections, thereby capturing global patterns. This method employs a GNN encoder for feature aggregation, while the pattern mining algorithm supervises the GNN training process through a novel loss function. Ref. [27] presents an anomaly detection scheme based on GAT and Informer. GAT effectively learns sequence features, while Informer excels in long-term sequence prediction. Their combined approach utilizes long-term prediction loss and short-term prediction loss to detect anomalies in multivariate time series.

However, these approaches only extract spatiotemporal features between individual temporal modalities across multiple WSN nodes, without addressing the extraction of correlation features among multiple temporal modalities across multiple nodes. Furthermore, most existing anomaly detection methods focus solely on collecting and analyzing temporal domain information. They primarily identify anomalous patterns through statistical characteristics, trend changes, or pattern matching in time series data. Consequently, these approaches overlook the importance of frequency domain information and fail to fully leverage the frequency domain features of data to enhance detection performance.

B. Frequency-Domain Analysis Approach for Anomaly Detection in WSNs

In the field of anomaly detection, frequency domain analysis has gained increasing attention as a crucial complementary approach. By transforming time-series data into the frequency domain, it reveals periodicity, frequency distribution, and the variation patterns of different frequency components. This information plays an indispensable role in understanding data correlation features and improving detection performance [23].

Currently, for WSN anomaly detection, existing research has extensively employed various typical frequency-domain analysis methods to reveal hidden periodic or frequency-based anomaly features. Among these, the Fourier Transform (FT), as the most commonly used frequency-domain tool, can rapidly map time-domain signals to the frequency domain, uncovering stable periodic patterns. It is frequently utilized to detect anomalies caused by periodic drift or noise interference. For instance, ref. [28] addresses sensor electrical signal acquisition in indoor environments. It employs the Fourier Transform to convert sensor-perceived signals from the time domain to the frequency domain, generating spatio-temporal image datasets.

> REPLACE THIS LINE WITH YOUR MANUSCRIPT ID NUMBER (DOUBLE-CLICK HERE TO EDIT) <

Combined with Generative Adversarial Networks (GANs), this approach detects anomalous behaviors within electrical signals. This method not only validates the effectiveness of frequency-domain information in anomaly detection for sensor-perceived signals but also demonstrates application potential in areas such as private space monitoring support and human activity perception. For multi-sensor signals of industrial gears, ref. [29] extracts frequency-domain features using the Fast Fourier Transform (FFT) and combines graph neural networks with adversarial autoencoders to achieve unsupervised anomaly detection. By mining multi-scale features within the frequency domain, this approach significantly enhances anomaly detection accuracy, validating the effectiveness of frequency-domain analysis in industrial multi-sensor scenarios.

In recent years, adaptive decomposition methods such as Empirical Mode Decomposition (EMD) have been introduced to decompose complex nonlinear non-stationary sequences into intrinsic mode functions. These frequency-domain methods partially overcome the limitations of single-time-domain analysis, which is sensitive to noise and struggles to capture periodic variations, providing an effective complementary approach for WSN anomaly detection. By integrating multivariate empirical mode decomposition with wavelet transform, ref. [30] addresses feature extraction challenges in vibration response data for environmental monitoring. Through signal decomposition followed by input into multiple deep learning models, it achieves efficient identification of damage types and locations within non-stationary signals, validating the practicality and high accuracy of combined EMD and time-frequency domain features for complex structural anomaly detection.

However, the aforementioned anomaly detection methods rely solely on frequency-domain processing, failing to fully leverage temporal domain information and thus limiting further performance improvements. Similarly, these approaches focus only on spatio-temporal feature extraction between single nodes with multiple modalities or between multiple nodes with a single modality, neglecting spatio-temporal correlations in scenarios involving multiple nodes and multiple modalities. This oversight impacts detection performance under complex anomaly conditions.

Based on the analysis of the aforementioned related work, this paper proposes a method called TE-MSTAD to address the limitations of existing WSN anomaly detection approaches. This method integrates both time-domain and frequency-domain information from the data for analysis and employs multiple information enhancement techniques to more comprehensively capture the spatial correlation features among multiple nodes. Furthermore, by incorporating a cross-modal feature extraction module based on an enhanced RWKV model, this approach can identify anomalies across different temporal modalities, thereby improving anomaly detection performance.

III. PROBLEM DESCRIPTION

This paper employs graph neural networks to model multi-temporal data (also termed multimodal data in literature)

collected by WSNs as dynamic attribute graphs, expressing their spatial correlations. Sensor nodes correspond to vertices in the graph, multi-temporal data collected by nodes correspond to attribute matrices, and sensor network topology connections correspond to edges in the attribute graph. Data collected by a wireless sensor network at timestamp t can be modeled as the attribute graph $\mathbf{G}_t = (\mathbf{X}_t, \mathbf{A}_t)$. Here, the attribute matrix $\mathbf{X}_t \in \mathbb{R}^{N \times M}$ represents M distinct modalities of data collected by N distinct WSN nodes. The value of an element a_{ij} in the adjacency matrix $\mathbf{A} \in \mathbb{R}^{N \times N}$ depends on the connection status between node i and node j . If an edge exists between node i and node j , then $a_{ij} = 1$; otherwise, $a_{ij} = 0$.

Considering a sequence of property graphs $\mathbf{G}[1:T] = (\mathbf{X}, \mathbf{A}) = \{\mathbf{G}_1, \mathbf{G}_2, \dots, \mathbf{G}_T\}$ over T time steps, where the property matrix is $\mathbf{X} = \{\mathbf{X}_1, \mathbf{X}_2, \dots, \mathbf{X}_T\}$ and the adjacency matrix is $\mathbf{A} = \{\mathbf{A}_1, \mathbf{A}_2, \dots, \mathbf{A}_T\}$, each $\mathbf{G}_t = (\mathbf{X}_t, \mathbf{A}_t)$ corresponds to the property graph at timestamp t . The anomaly detection problem for WSN time-series data can then be formulated as a classification task for property graphs. Designing an appropriate neural network architecture and its weight parameters θ , we define the corresponding mapping function f as:

$$\mathbf{Y} = f(\mathbf{G}[t_1 : t_1 + W] | \theta) \in (0, 1)^{N \times M \times W} \quad (1)$$

A collection of temporal attribute graphs $\mathbf{G}[t_1 : t_1 + W]$ formed by data collected by WSN within the time window from t_1 to $t_1 + W$. \mathbf{Y} is a label matrix with shape $N \times M \times W$, corresponding to the output matrix of N nodes across M modalities within a time window of length W . $y_t^{i,j}$ represents the label for the j th modality at node i at time t . When $y_t^{i,j}$ is 1, the target modality at the target node exhibits an anomaly at this time; when $y_t^{i,j}$ is 0, the target modality at the target node behaves normally at this time.

IV. MODEL DESIGN

The proposed TE-MSTAD anomaly detection model structure is illustrated in Fig. 1, comprising a data preprocessing module, a topology information learning module, a time-domain feature extraction module, and a frequency-domain feature extraction module. This model adopts a dual-branch reconstruction architecture to perform anomaly detection on both the time-domain and frequency-domain features of signals. On one hand, the time-domain branch captures temporal characteristics within the time series. On the other hand, the frequency-domain branch utilizes spectral analysis to uncover periodic and latent frequency features. These two branches work collaboratively to achieve more comprehensive anomaly detection performance.

After preprocessing the WSN-collected dataset, the topology learning module acquires the topo-logical relationships

> REPLACE THIS LINE WITH YOUR MANUSCRIPT ID NUMBER (DOUBLE-CLICK HERE TO EDIT) <

between nodes, deriving their adjacency matrix and constructing an attribute graph. Subsequently, the time series data undergoes wavelet transformation to extract frequency domain information, including amplitude and phase, forming a frequency matrix. The processed data is then input into the model's two branches. In the time-domain branch, the original time series undergoes encoding to extract temporal features and spatio-temporal correlations. These are then reconstructed via a

decoder to produce a time-reconstructed sequence. Simultaneously, the frequency matrix enters the frequency-domain branch, where a similar encoding-decoding process extracts its frequency-domain features and completes reconstruction. Ultimately, the model achieves comprehensive anomaly detection across both time and frequency domains through its dual-branch reconstruction mechanism.

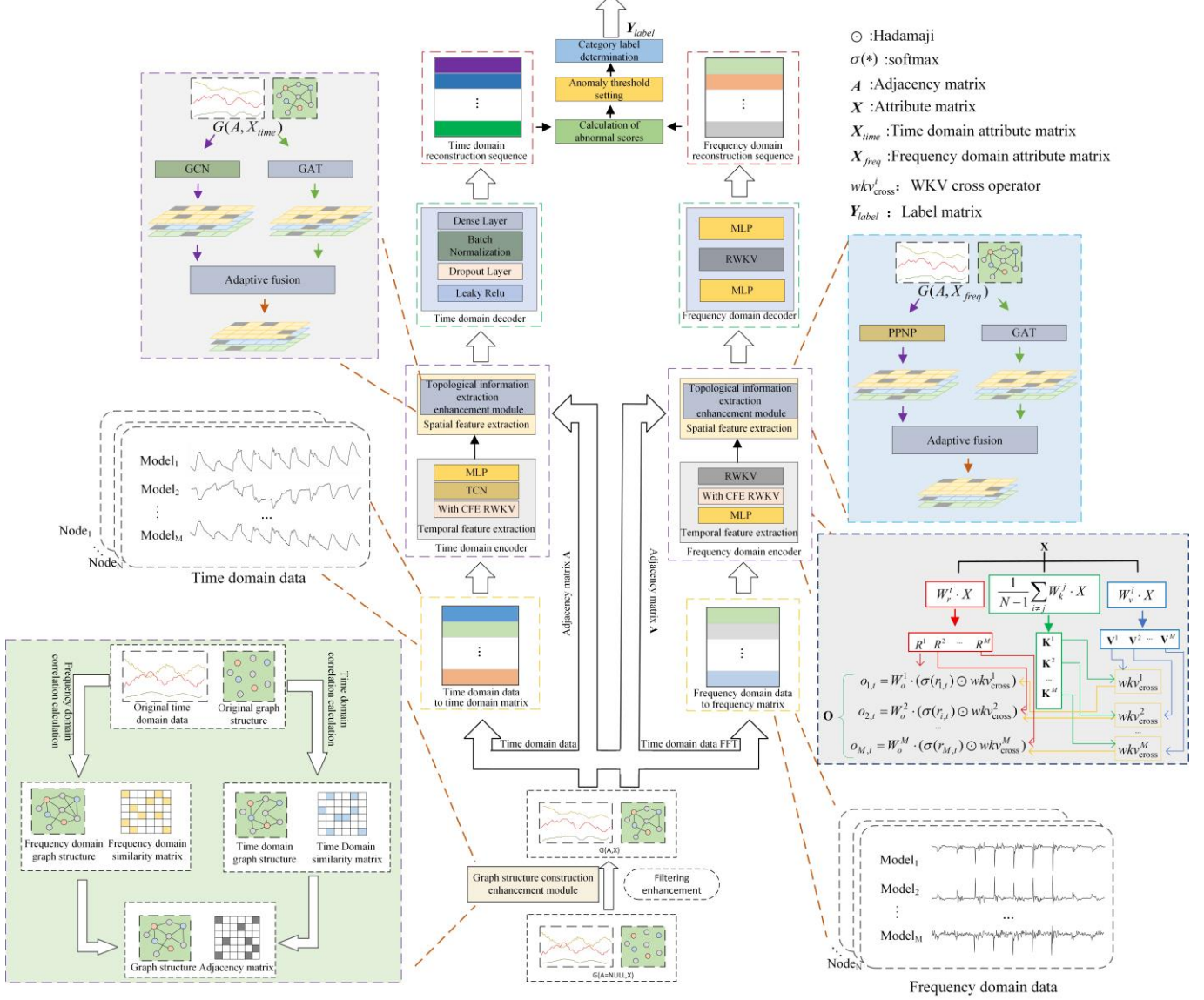


Fig. 1. Block diagram of the TE-MSTAD model.

A. Data Preprocessing

The data preprocessing module transforms raw data collected by WSNs into training samples suitable for the model, primarily involving three steps: filtering, downsampling, and normalization.

First, WSN-collected data typically contains substantial high-frequency natural noise originating from environmental interference, hardware components, and other factors. This noise includes large amounts of useless or even misleading information that can interfere with the model's extraction of key features, thereby affecting anomaly detection performance.

Therefore, in order to effectively suppress high-frequency noise, this module applies a Gaussian filter in the frequency domain to obtain a smoothed time-domain signal $\tilde{x}(t)$ after filtering.

Subsequently, to reduce redundancy in the raw data, this paper employs a sliding window mechanism for time series downsampling after completing Gaussian filtering noise reduction in the frequency domain. This method segments continuous time series data by setting a sliding step size k and window length kW . Let the current time be t . Starting from this point, kW data points form a

time series sample of length kW , denoted as $\tilde{\mathbf{x}}_{raw} = [\mathbf{x}_t, \mathbf{x}_{t+1}, \dots, \mathbf{x}_{t+kW-1}] \in \mathbb{R}^{M \times N \times kW}$. After sliding window subsampling, the data $\tilde{\mathbf{x}}_{raw}$ is divided into k subsamples. Each subsample can be regarded as an observation sequence for a node: $\mathbf{X}_i \in \mathbb{R}^{M \times N \times W}$, $i \in [1, k]$.

Finally, to eliminate differences in dimensionality and numerical ranges between sensor data and enhance model training stability and convergence speed, this paper applies standardization to the data after downsampling. The commonly used Z-Score standardization method is employed. By subtracting the mean and dividing by the standard deviation for each data point, it is transformed into a standard normal distribution with mean 0 and standard deviation 1, thereby achieving a unified numerical scale. The specific procedure is as follows:

$$\tilde{\mathbf{X}}_{i,j} = (\mathbf{X}_{i,j} - \mu(\mathbf{X}_{i,j})) / \sigma(\mathbf{X}_{i,j}) \quad (2)$$

where $\mathbf{X}_{i,j}$ is the input data after downsampling of the j th mode of the i th node; $\mu(\mathbf{X}_{i,j})$ represents the mean value of $\mathbf{X}_{i,j}$ over the entire time series; $\sigma(\mathbf{X}_{i,j})$ denotes the standard deviation of $\mathbf{X}_{i,j}$; and $\tilde{\mathbf{X}}_{i,j}$ is the processed standardized result.

B. Spatial Correlation Feature Learning Enhancement Module

Following the data preprocessing module, this paper designs and introduces a joint time-frequency domain feature correlation learning enhancement algorithm. This algorithm aims to fully explore the spatial correlations among nodes in wireless sensor networks within the time-frequency domain, thereby constructing a more reasonable graph structure to enhance the model's ability to represent topological information.

Specifically, this module first maps the time-domain observation data $\mathbf{X}_{time} \in \mathbb{R}^{M \times N \times W}$ of sensor nodes to the frequency domain via Fourier transform, yielding the frequency-domain feature matrix $\mathbf{X}_{freq} \in \mathbb{R}^{M \times N \times W}$.

Next, to measure spatial correlation between nodes, this paper employs the Spearman correlation coefficient. The average correlation value across three modalities serves as the basis for constructing the adjacency matrix for each node. For any two nodes a and b , their correlation in the j th modality is calculated as follows:

$$\rho_{a,b}^j = \frac{\text{cov}(r(\mathbf{X}_{a,j}), r(\mathbf{X}_{b,j}))}{\sigma(r(\mathbf{X}_{a,j})) \cdot \sigma(r(\mathbf{X}_{b,j}))} \quad (3)$$

where $\rho_{a,b}^j$ denotes the Spearman rank correlation coefficient between nodes a and b , in the j th mode; $r(\bullet)$ represents the rank transformation applied to the sequence; $\text{cov}(\bullet)$ and $\sigma(\bullet)$ denote the covariance and standard deviation operations, respectively.

Subsequently, the correlations within each modality in the time domain and frequency domain are averaged separately. The correlation values from the three modalities are then

aggregated to obtain the node's overall correlation score:

$$S_{a,b} = \frac{1}{2N} \sum_{n=1}^N (\rho_{a,b}^{(time,n)} + \rho_{a,b}^{(freq,n)}) \quad (4)$$

where $S_{a,b}$ represents the joint correlation score between node a and node b ; N denotes the number of modalities within a single node; $\rho_{a,b}^{(time,n)}$ and $\rho_{a,b}^{(freq,n)}$ denote the data correlation in the time domain and frequency domain, respectively, for the corresponding node in the n th modality.

Finally, to construct a sparse and discriminative adjacency matrix $\mathbf{A} \in \mathbb{R}^{N \times N}$, this paper employs a Top K strategy to select the top k most relevant nodes for each node. Corresponding elements are set to 1, while all others are set to 0, thereby building an adaptive graph structure:

$$A_{a,b} = \begin{cases} 1, & \text{if } S_{a,b} \in TopK(S_{a,:}) \\ 0, & \text{otherwise} \end{cases} \quad (5)$$

where $TopK(S_{a,:})$ denotes the top K nodes most correlated with node a ; $A_{a,b}$ represents the elements in the adjacency matrix \mathbf{A} .

C. Time-Domain Feature Extraction Network Branch

In the temporal feature extraction branch, the model takes the attribute matrix $\mathbf{X}_{time} \in \mathbb{R}^{B \times M \times N \times W}$ and adjacency matrix $\mathbf{A} \in \mathbb{R}^{N \times N}$ —both processed into batches of size B —as inputs. The temporal encoder extracts temporal and spatial correlations from the input data, compressing them into a low-dimensional representation. Subsequently, the temporal decoder decodes and reconstructs the encoded representation, aiming to restore the original input sequence as faithfully as possible. The encoder and decoder work in tandem, enabling the model to capture critical temporal features. Next, we will provide a detailed introduction to the specific structure and functions of the temporal encoder module and the temporal decoder module.

As shown in Fig. 1, within the temporal domain encoder module, the input temporal domain data sequentially passes through the temporal feature extraction component and the spatial feature extraction component. The temporal feature extraction component is responsible for uncovering temporal correlations in node attributes over time while capturing intermodal correlations among different physical quantities. The spatial feature extraction component, meanwhile, extracts spatial correlations within the network topology.

The RWKV model is a sequence modeling framework that combines the strengths of RNNs and Transformers, featuring linear time complexity and suitability for long text processing [19]. Composed of stacked residual blocks, it incorporates temporal mixing sub-blocks and channel mixing sub-blocks. By introducing a recursive structure, it fully leverages past information.

The temporal mixing sub-block of the RWKV model primarily handles temporal dependencies in sequence data. It efficiently fuses information from the current time step with states from historical time steps through a recursive update

> REPLACE THIS LINE WITH YOUR MANUSCRIPT ID NUMBER (DOUBLE-CLICK HERE TO EDIT) <

mechanism, enabling feature extraction from long sequences:

$$\begin{aligned}
 \mathbf{x}_{\text{mix}} &= \lambda_{\text{time_mix}} \cdot \mathbf{x}_t^{\text{in}} + (1 - \lambda_{\text{time_mix}}) \cdot \mathbf{x}_{t-1}^{\text{in}} \\
 \mathbf{r}_t &= \mathbf{W}_r \cdot \mathbf{x}_{\text{mix}} \\
 \mathbf{k}_t &= \mathbf{W}_k \cdot \mathbf{x}_{\text{mix}} \\
 \mathbf{v}_t &= \mathbf{W}_v \cdot \mathbf{x}_{\text{mix}} \\
 \mathbf{wkv}_t &= \frac{\sum_{i=1}^{t-1} e^{-(t-1-i)w+k_i} \odot \mathbf{v}_i + e^{u+k_t} \odot \mathbf{v}_t}{\sum_{i=1}^{t-1} e^{-(t-1-i)w+k_i} + e^{u+k_t}} \\
 \mathbf{o}_t &= \mathbf{W}_o \cdot (\sigma(\mathbf{r}_t) \odot \mathbf{wkv}_t)
 \end{aligned} \tag{6}$$

where the input is the sequence $\mathbf{x}_t^{\text{in}} \in \mathbb{R}^d$, $\lambda_{\text{time_mix}}$ is a learnable vector; $\mathbf{W}_r, \mathbf{W}_k, \mathbf{W}_v \in \mathbb{R}^{d \times d}$ is the linear weight; \mathbf{k}_i and \mathbf{v}_i are the K-vector and V-vector at the i th time step; $u \in \mathbb{R}^d$ is a learnable log decay parameter controlling the degree of historical retention; \mathbf{wkv}_t is a weighted sum similar to attention but without Q or quadratic matrix multiplication, resulting in low computational cost. \mathbf{W}_o is a learnable linear projection matrix; σ is the Sigmoid function controlling the information pass rate; \odot represents element-wise multiplication; \mathbf{o}_t is the tensor output from the temporal mixing module.

The channel mixing subblock in the RWKV model primarily enhances the feature expression capability of sequence representations. It models inter-channel dependencies by applying nonlinear transformations and combining different feature channels of the input sequence, thereby extracting richer, higher-dimensional semantic information.

In the TE-MSTAD network model, the time-domain embedding vector $\mathbf{X}_{\text{time}} \in \mathbb{R}^{B \times N \times W \times M}$ is first fed into the enhanced RWKV network for processing. To effectively extract correlations across modalities, this paper introduces a cross-extraction block based on the RWKV temporal mixing component. This cross-extraction block employs a mechanism analogous to cross-attention. For the i th modal feature, its own V vector undergoes cross-computations with the K vectors generated by other modalities, producing WKV operators $\mathbf{wkv}_{\text{cross}}^i$ containing cross-modal information. Subsequently, the R vector of this feature is computed with the operator $\mathbf{wkv}_{\text{cross}}^i$, yielding an output that fuses information across different modalities:

$$\begin{aligned}
 \mathbf{X}_{\text{mix}} &= \lambda_{\text{time_mix}} \cdot \mathbf{X}_{t,\text{time}} + (1 - \lambda_{\text{time_mix}}) \cdot \mathbf{X}_{t-1,\text{time}} \\
 \mathbf{r}_{i,t} &= \mathbf{W}_r^i \cdot \mathbf{X}_{\text{mix}} \\
 \mathbf{v}_{i,t} &= \mathbf{W}_v^i \cdot \mathbf{X}_{\text{mix}} \\
 \mathbf{k}_{\text{cross}}^{i,t} &= \frac{1}{N-1} \sum_{i \neq j} \mathbf{W}_k^j \cdot \mathbf{X}_{\text{mix}} \\
 \mathbf{wkv}_{\text{cross}}^i &= \frac{\sum_{i=1}^{t-1} e^{-(t-1-i)w+k_{\text{cross}}^i} \odot \mathbf{v}_i + e^{u+k_{\text{cross}}^{i,t}} \odot \mathbf{v}_t}{\sum_{i=1}^{t-1} e^{-(t-1-i)w+k_{\text{cross}}^i} + e^{u+k_{\text{cross}}^{i,t}}} \\
 \mathbf{o}_{i,t} &= \mathbf{W}_o^i \cdot (\sigma(\mathbf{r}_{i,t}) \odot \mathbf{wkv}_{\text{cross}}^i)
 \end{aligned} \tag{7}$$

The above formula represents an improvement over Eq. 6. Here, the superscript $i, j \in [1, M], i \neq j$ denotes the sequence numbers of two distinct modalities. $\mathbf{X}_{t-1,\text{time}} \in \mathbb{R}^{B \times N \times 1 \times d_i}$ corresponds to the data from modality i within the input tensor $\mathbf{X}_{t-1,\text{time}} \in \mathbb{R}^{B \times N \times W \times d_{in}}$ to the CFE block. $d_{in} = \sum_{i=1}^M d_i$ and d_i denote the feature dimensions of modality i . $\mathbf{k}_{\text{cross}}^{i,t}$ is the K-vector obtained by cross-mapping \mathbf{X}_{mix} through the learnable matrix \mathbf{W}_k^j corresponding to the remaining modality features. The output $\mathbf{k}_{\text{cross}}^{i,t}$ is derived by averaging the product of the temporal mixed input tensor $\mathbf{X}_{\text{mix}} \in \mathbb{R}^{B \times N \times 1 \times d_i}$ and the mapping matrix $\mathbf{W}_k^j \in \mathbb{R}^{d_i \times d}$ corresponding to other distinct modalities. This cross-modal operation enables information fusion across modalities and establishes intermodal correlations. $\mathbf{wkv}_{\text{cross}}^i$ represents the WKV operator generated using $\mathbf{k}_{\text{cross}}^{i,t}$; $\mathbf{o}_{i,t}$ denotes the output of the temporal mixing component, which is subsequently fed into the channel mixing part of RWKV and concatenated to produce the output vector $\mathbf{X}_{\text{rwkv}^*} \in \mathbb{R}^{B \times N \times W \times M}$, where the subscript denotes the improved RWKV model.

To further extract temporal features and perform dimensionality reduction, this model explored multiple network architectures, ultimately incorporating a Temporal Convolutional Network (TCN) and Multi-Layer Perceptron (MLP) structure. The TCN consists of a series of causal convolutional layers with dilation rates, enabling the capture of temporal dependencies across different scales. The MLP facilitates dimension reduction during encoding, feeding low-dimensional embedding vectors to the decoder. Its primary computation can be represented as:

$$\mathbf{X}_{\text{TCN}}^{(l)} = \text{ReLU}(\mathbf{y}_t^{(l)} + \mathbf{x}_t^{(l-1)}) \tag{8}$$

where, in TCN, $\mathbf{y}_t^{(l)}$ is the output of the dilated convolution operation at time step t in layer l ; \mathbf{X}_{TCN} represent the final output tensors of the TCN.

After completing feature extraction and dimensionality reduction for temporal features, the attribute matrix output $\mathbf{X}_{\text{MLP}} \in \mathbb{R}^{B \times N \times W \times d_{\text{MLP}}}$ by the MLP serves as the node feature

> REPLACE THIS LINE WITH YOUR MANUSCRIPT ID NUMBER (DOUBLE-CLICK HERE TO EDIT) <

input. This is combined with the adjacency matrix $\mathbf{A} \in \mathbb{R}^{N \times N}$ generated by the topology information learning module and jointly fed into the spatial feature extraction module. This module integrates two types of graph neural network submodels: graph convolutional network (GCN) and graph attention network (GAT). GCN performs mean aggregation of neighbor node features using a static adjacency matrix, offering high modeling efficiency and strong global structural modeling capabilities. GAT, on the other hand, introduces an attention mechanism that assigns different weights to distinct adjacent nodes, enabling more refined feature representation. Combining GCN and GAT as an information enhancement approach balances global structural stability with local feature adaptability, enhancing the model's ability to capture complex spatial dependencies.

Subsequently, this paper performs adaptive integration of the outputs from GCN and GAT, ultimately expressed as:

$$\mathbf{H}_{\text{spatial}} = \lambda \cdot \mathbf{H}_{\text{GAT}} + (1 - \lambda) \cdot \mathbf{H}_{\text{GCN}} \quad (9)$$

where the fusion coefficient $\lambda \in [0,1]$ is a trainable parameter.

It is adaptively adjusted through model training to determine the contribution ratio of the two submodels to the final representation.

In the network architecture designed herein, the temporal decoder sequentially incorporates a Dense Layer, Batch Normalization, a Dropout Layer, and a Leaky ReLU activation function. These modules not only perform dimensionality-increasing decoding on the feature matrix but also enhance training stability and mitigate overfitting risks, thereby accomplishing feature reconstruction during the decoding phase. First, the Dense Layer performs a linear mapping on the temporal-encoded features to achieve dimensionality expansion. Subsequently, Batch Normalization is introduced to mitigate internal covariate shifts, accelerate model convergence, and enhance stability during mini-batch training. To improve generalization and prevent overfitting, a Dropout Layer is then incorporated into the decoder. During each training iteration, the dropout layer randomly masks the activation values of some neurons with probability p . Finally, Leaky ReLU is selected as the nonlinear activation function to avoid the "neuron death" phenomenon that may occur in the negative range with standard ReLU.

D. Frequency Domain Feature Extraction Module

In the feature extraction module of the frequency domain, the input data $\mathbf{X}_{\text{time}} = \{\mathbf{X}_1, \mathbf{X}_2, \dots, \mathbf{X}_T\}$ is first mapped to the frequency domain space via Fast Fourier Transform (FFT), yielding the frequency domain tensor $\mathbf{X}_{\text{freq}} = \{\mathbf{F}_1, \mathbf{F}_2, \dots, \mathbf{F}_T\}$.

The time-frequency transformation process is as follows:

$$f_{\alpha, \beta}^{(k)} = \sum_{t=1}^T x_{\alpha, \beta}^{(t)} \left(\cos\left(\frac{2\pi tn}{T}\right) - i \sin\left(\frac{2\pi tn}{T}\right) \right) \quad (10)$$

where i denotes the imaginary part, $i^2 = -1$; $x_{\alpha, \beta}^{(t)}$ represents the time series corresponding to the mode β of node α in

\mathbf{X}_{time} , with the superscript $t \in [1, T]$; similarly, $f_{\alpha, \beta}^{(k)}$ corresponds to the frequency domain sequence mapped from $x_{\alpha, \beta}^{(t)}$. However, since $f_{\alpha, \beta}^{(k)}$ is a complex sequence, it cannot be directly used for training neural network models. To address this issue, the frequency domain information is typically decomposed into amplitude and phase components for separate representation and storage. Specifically, for the frequency domain sequence $f_{\alpha, \beta}^{(k)}$, the amplitude can be understood as the Euclidean distance of this complex number from the origin in the complex plane, while the phase represents the angle formed with the positive real axis in the complex plane. Assuming $f_j(k) = m + ni$, where m and n denote the real and imaginary parts respectively, the amplitude a and phase p are calculated as follows:

$$\begin{aligned} a &= \sqrt{m^2 + n^2} \\ p &= \arctan(m/n) \end{aligned} \quad (11)$$

By calculating the magnitude and phase of each complex element in the frequency domain sequence $f_{\alpha, \beta}^{(k)}$, the original complex sequence can be transformed into two real-valued sequences suitable for model training: the magnitude sequence \mathbf{a}_k and the phase sequence \mathbf{p}_k . Similarly, for each input sample set $\{\mathbf{X}_1, \mathbf{X}_2, \dots, \mathbf{X}_T\}$, after undergoing the time-frequency domain transformation, the magnitude matrix $\mathbf{A} \in \mathbb{R}^{N \times W \times M}$ and the phase matrix $\mathbf{P} \in \mathbb{R}^{N \times W \times M}$ can be obtained. These two matrices are concatenated and divided into batches to form the frequency-domain matrix $\mathbf{X}_{\text{freq}} \in \mathbb{R}^{B \times N \times 2W \times M}$, which serves as input to the frequency-domain encoding network. This enables the encoder to effectively extract sample features based on frequency-domain information.

As shown in Fig. 1, similarly to the temporal domain encoder module, the input temporal domain data sequentially passes through the temporal feature extraction and spatial feature extraction components. The temporal embedding vector $\mathbf{X}_{\text{freq}} = \{\mathbf{F}_1, \mathbf{F}_2, \dots, \mathbf{F}_T\} \in \mathbb{R}^{B \times N \times 2W \times M}$ first traverses a MLP network for dimensionality reduction and nonlinear feature mapping. Subsequently, to extract intermodal correlations, the output feature $\mathbf{H}^{(1)}$ is further fed into an enhanced RWKV model. This module incorporates a CFE block. After thorough extraction of temporal dependency features, the output features are input into the RWKV network for the extraction of temporal features:

$$\begin{aligned} \mathbf{H}^{(1)} &= \text{MLP}(\mathbf{X}_{\text{freq}}) \in \mathbb{R}^{B \times N \times 2W \times d_1} \\ \mathbf{H}^{(2)} &= \text{RWKV}^*(\mathbf{H}^{(1)}) \in \mathbb{R}^{B \times N \times 2W \times d_2} \\ \mathbf{H}^{(3)} &= \text{RWKV}(\mathbf{H}^{(2)}) \in \mathbb{R}^{B \times N \times 2W \times d_3} \end{aligned} \quad (12)$$

where the superscript denotes the reduced dimension after dimension reduction d_1, d_2, d_3 ; $\mathbf{H}^{(1)}, \mathbf{H}^{(2)}, \mathbf{H}^{(3)}$ represents the

output tensor after processing through each network; and RWKV* denotes the improved RWKV model.

After completing the temporal feature extraction and dimensionality reduction of the frequency-domain embedding vectors, the frequency-domain attribute matrix $\mathbf{H}^{(3)}$ output by the MLP serves as the node feature representation. Combined with the adjacency matrix $\mathbf{A} \in \mathbb{R}^{N \times N}$ generated by the topology learning module, these are jointly input into the frequency-domain spatial feature extraction module to further learn the spatial dependencies between nodes in the frequency domain. To fully exploit both local and global spatial structural information, this paper introduces two complementary graph neural network submodels in the frequency-domain spatial feature extraction component: the propagatable approximation Personalized Propagation of Neural Predictions (PPNP) and the Graph Attention Network (GAT). Each focuses on learning spatial features at distinct levels, and through subsequent adaptive weighted fusion, they jointly generate frequency-domain feature representations enriched with spatial information.

First, the PPNP subnetwork employs the Personalized PageRank (PPR) propagation mechanism to smoothly transmit node information across the entire graph. This balances the need for both local neighborhood information and broader neighborhood insights, enabling the model to capture more stable spatial structural dependencies even in sparse or noisy networks. Its core propagation process can be formalized as:

$$\begin{aligned} \mathbf{H}_{\text{PPNP}} &= \alpha(\mathbf{I} - (1-\alpha)\hat{\mathbf{A}})^{-1}\mathbf{H}^{(3)}\mathbf{W}_{\text{PPNP}} & (13) \\ \hat{\mathbf{A}} &= \mathbf{D}^{-1/2}\mathbf{A}\mathbf{D}^{-1/2} \end{aligned}$$

where α is an adjustable propagation coefficient, $\hat{\mathbf{A}}$ is the symmetric normalized adjacency matrix, \mathbf{D} is the node degree matrix, and \mathbf{W}_{PPNP} is the learnable weight matrix. This propagation process effectively suppresses local noise interference in node representations and enhances global consistency of features.

In contrast, the GAT subnetwork introduces an adaptive attention mechanism to assign different weights to distinct neighboring nodes, focusing on modeling dependencies among local neighbors:

$$\mathbf{H}_{\text{GAT}} = \text{GAT}(\mathbf{H}^{(3)}) \quad (14)$$

Finally, the spatial features extracted by the PPNP and GAT subnetworks undergo adaptive weight fusion in the channel dimension. This approach not only effectively captures the complex spatial relationships between nodes in the frequency domain but also enhances the accuracy and generalization capability of anomaly detection in complex network environments. represents the adaptive learning fusion weight, with the process expressed as:

$$\mathbf{H}_{\text{freq}}^{\text{spatial}} = \beta \cdot \mathbf{H}_{\text{PPNP}} + (1-\beta) \cdot \mathbf{H}_{\text{GAT}} \quad (15)$$

In the network architecture designed herein, the frequency-domain decoder section first introduces an MLP to perform nonlinear mapping and dimension recovery on the results extracted from the frequency-domain spatial features.

Following the initial feature dimensionality expansion by the MLP, the frequency-domain decoder further incorporates an RWKV module to leverage its strengths in modeling long-range temporal dependencies. Finally, to effectively map the RWKV output tensor back to the feature space consistent with the original input, the decoder applies another MLP module for output refinement. Overall, the frequency-domain decoder employs an "MLP-RWKV-MLP" structural combination to ensure thorough restoration and reconstruction of frequency-domain features during decoding, providing an accurate and reliable reconstruction foundation for anomaly detection results.

E. Anomaly Score

The anomaly detection method proposed in this study employs reconstruction error as the anomaly discrimination criterion, adhering to the design philosophy of autoencoder-like frameworks[31]. During training, the model aims to minimize the discrepancy between reconstructed outputs and observed input data, leveraging this discrepancy to quantify whether anomalies exist in the input data. Considering the reconstructed outputs generated in both the time domain and frequency domain after the input data passes through the network model, they are denoted respectively as:

The reconstructed outputs generated in the time domain and frequency domain after the input data passes through the network model are denoted as $\hat{\mathbf{X}}_{\text{time}}$ and $\hat{\mathbf{X}}_{\text{freq}}$, respectively, with their corresponding original inputs being \mathbf{X}_{time} and \mathbf{X}_{freq} . Additionally, the frequency-domain reconstruction result $\hat{\mathbf{X}}_{\text{freq}}$ can be restored to time-domain form $\mathcal{F}^{-1}(\hat{\mathbf{X}}_{\text{freq}})$ via inverse Fourier transform \mathcal{F}^{-1} , enabling comparison with \mathbf{X}_{time} . Therefore, to comprehensively consider these three reconstruction errors, three loss functions are defined as follows:

$$\begin{aligned} \mathcal{L}_1 &= \frac{1}{WNM} \sum_{t=1}^W \sum_{i=1}^N \sum_{j=1}^M \left\| \hat{\mathbf{X}}_{\text{time}}^{(i,j,t)} - \mathbf{X}_{\text{time}}^{(i,j,t)} \right\|_2^2 \\ \mathcal{L}_2 &= \frac{1}{2WNM} \sum_{t=1}^{2W} \sum_{i=1}^N \sum_{j=1}^M \left\| \hat{\mathbf{X}}_{\text{freq}}^{(i,j,t)} - \mathbf{X}_{\text{freq}}^{(i,j,t)} \right\|_2^2 \\ \mathcal{L}_3 &= \frac{1}{WNM} \sum_{t=1}^W \sum_{i=1}^N \sum_{j=1}^M \left\| \mathcal{F}^{-1}(\hat{\mathbf{X}}_{\text{freq}}^{(i,j,t)}) - \mathbf{X}_{\text{time}}^{(i,j,t)} \right\|_2^2 \end{aligned} \quad (16)$$

To fully leverage both time-domain and frequency-domain information while adaptively weighting the influence of different loss terms, this paper introduces an attention-based weighting mechanism. Each loss term is assigned distinct weight coefficients via a softmax operation. Let the weight coefficients be denoted as $\alpha_1, \alpha_2, \alpha_3$. The final total loss function and anomaly score are then expressed as:

$$\text{score}_t(i, j) = \mathcal{L}_{\text{total}} = \alpha_1 \cdot \mathcal{L}_1 + \alpha_2 \cdot \mathcal{L}_2 + \alpha_3 \cdot \mathcal{L}_3 \quad (22)$$

A higher anomaly score indicates greater deviation between the input data and the model prediction at that time point, making it more likely to be classified as an anomaly. By setting a threshold τ based on the final loss entropy value during model training, we can determine whether a specific time point

is anomalous. When $score_t(i, j)$ exceeds the threshold τ , the data is classified as anomalous and labeled as 1; otherwise, it is classified as non-anomalous and labeled as 0.

$$y_t(i, j) = \begin{cases} 1, & score_t(i, j) > \tau \\ 0, & score_t(i, j) \leq \tau \end{cases} \quad (17)$$

V. EXPERIMENTAL ANALYSIS

A. Dataset and Parameter Settings

To comprehensively evaluate the performance and adaptability of the anomaly detection model proposed in this paper, experimental validation was conducted on both public datasets and real-world collected datasets. As shown in Fig. 2, the public dataset consists of WSN data collected and compiled by Intel Berkeley Research Lab through deploying multiple wireless sensor nodes (Intel Berkeley Research Lab datasets, IBRL). This dataset comprises 54 Mica2Dot sensor nodes, each collecting environmental data such as temperature, humidity, light intensity, and voltage every 31 seconds. As illustrated in Fig. 3, the real-world dataset was generated by constructing a WSN data collection system suitable for outdoor scenarios based on the LoRa communication protocol. This system consists of 14 distributed sensor nodes and one aggregation node. All sensor nodes were deployed in an open outdoor area, arranged sequentially along a perimeter wall at a uniform height of 35 centimeters above ground level. The aggregation node centrally receives data from all sensors and transmits it via WiFi to a cloud-based data center for remote data transmission and management. Each sensor node collects temperature, humidity, and voltage parameters every 30 seconds. The resulting dataset, named LoRA-OSD, covers the time period from November 26, 2024, to January 7, 2025, documenting environmental monitoring information during this phase.

The experimental platform configuration used in this study is as follows: the processor is an Intel® Xeon® Gold5218CPU@2.30GHz, the graphics processing unit is an NVIDIA GeForce RTX 3090, and the operating system is Ubuntu 18.04.2 LTS. The experimental environment was developed using Python 3.6.9, employing the PyTorch 2.0.0 deep learning framework and integrating CUDA 11.7 for GPU-accelerated computation. During subsequent debugging experiments, the learning rate was set to lr=0.0002, training epochs to epoch=120, sliding window size to W=200, sliding stride to L=150, and the Adam optimizer was employed.

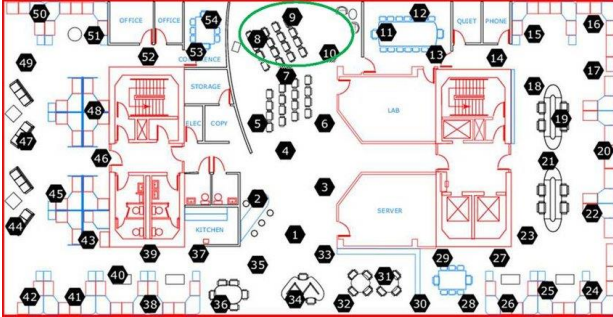


Figure 2. Spatial position distribution map of sensor nodes in the IBRL dataset.



(a) Node distribution map. (b) Sensor node.
Fig. 3. Deployment of sensor nodes in the WSN abnormal node detection system.

B. Evaluation Metrics

To comprehensively evaluate the performance of the proposed anomaly detection model, this paper selects Precision, Recall, and F1-score as the primary evaluation metrics. Let TP (True Positives) denote the number of samples correctly identified as anomalies, FP (False Positives) denote the number of normal samples incorrectly identified as anomalies, FN (False Negatives) denote the number of anomalies not detected, and TN (True Negatives) denote the number of samples correctly identified as normal

Precision measures the proportion of samples correctly classified as anomalies (True Positives, TP) among all samples predicted as anomalies (True Positives + False Positives, TP + FP). A high precision indicates fewer false positives and higher predictive reliability. Its formula is:

$$\text{Precision} = \frac{TP}{TP + FP} \quad (18)$$

Recall measures the proportion of actual anomalies (TP + FN) that are correctly identified by the model. A high recall indicates fewer false negatives and stronger detection capability. Its formula is:

$$\text{Recall} = \frac{TP}{TP + FN} \quad (19)$$

The F1-score is the harmonic mean of precision and recall, serving as a balanced, comprehensive evaluation metric between these two indicators. The F1-score unifies precision and recall into a single metric. Its formula is:

$$F1 = \frac{2 \times \text{Precision} \times \text{Recall}}{\text{Precision} + \text{Recall}} \quad (20)$$

C. Ablation Experiments

To evaluate the role and performance of each module in the proposed network model, corresponding ablation experiments were designed and conducted. In these experiments, multiple ablation schemes were established, removing or modifying specific key modules within the network model to assess their actual impact on overall performance. The following ablation schemes were designed:

Scheme 1: Remove the CE module that extracts intermodal correlations, reverting to the original RWVK model.

Scheme 2: Modify the topology information enhancement method to use only GAT networks in both the time and frequency domains.

Scheme 3: Modify the topology learning enhancement method to compute correlations only in the temporal domain to

obtain the adjacency matrix.

Scheme 4: Simultaneously modify both the topology information enhancement method and the topology learning enhancement method. Use only the GAT network on both the time-frequency domain branch and the time domain branch, and employ the adjacency matrix computed solely in the time domain.

Scheme 5: Remove the frequency domain branch after attribute matrix input, perform feature extraction solely in the time domain, and complete both reconstruction and anomaly detection.

Scheme 6: Remove the time-domain branch after attribute matrix input, perform feature extraction solely in the frequency domain, and complete both the reconstruction and anomaly detection tasks.

Scheme 7: Use the complete model designed in this paper without any removal or modification.

TABLE I.
ABLATION STUDY PROTOCOLS AND RESULTS

Scheme	Precision	Recall	F1 Score
1	86.53%	78.35%	82.24%
2	90.05%	84.53%	87.18%
3	91.12%	86.61%	89.81%
4	89.66%	82.27%	85.81%
5	89.94%	79.51%	84.41%
6	89.10%	76.41%	82.27%
7	91.04%	94.09%	92.52%

The experimental results for different ablation schemes are shown in Table I. Since scheme 1 removed the CFE module, the RWKV model in the experiment could not effectively mine potential correlation features between multimodal data and lost its ability to extract multimodal correlations. Therefore, compared to the baseline model (Scheme 7), the model in this scheme overlooked a significant number of intermodal correlation anomalies during detection, resulting in decreases of 4.51%, 15.74%, and 10.28% in precision, recall, and F1 score, respectively. In scheme 2, both the temporal and spatial domains of the model employ a single GAT for spatial feature extraction, failing to fully leverage the strengths and complementarity of different submodels. Compared to the baseline model, the F1 score decreased by 5.34%, while precision and recall dropped by 0.99% and 9.56%, respectively. This indicates that a single graph neural network architecture has limitations in extracting topological features and fails to adequately detect anomalies between nodes. Scheme 3 restricted the construction of the adjacency matrix to time-domain information only, neglecting hidden features in the frequency domain. The F1 score decreased by approximately 2.71%, indicating that phase, frequency, and other information in the frequency domain can significantly enhance the node association patterns captured by the adjacency matrix, thereby improving the quality of spatial structure learning. Scheme 4 simultaneously modifies both information enhancement methods of the model: it removes the ensemble approach for multiple submodels in the topological information enhancement and simplifies the adjacency matrix construction to rely solely on temporal correlations. Experimental results show that compared to the baseline model, the F1 score

decreased by 6.71%. This indicates a noticeable decline in overall model performance, validating the synergistic role of both topological information enhancement approaches in improving anomaly detection capabilities. Schemes 5 and 6, which removed the frequency domain or time domain branch respectively, exhibited significant deficiencies in information capture, resulting in F1 score decreases of 8.11% and 10.25%. This demonstrates that a single-branch structure struggles to comprehensively capture the latent time-frequency feature information within the data. As the complete model, scheme 7 integrates multimodal modeling, topological information enhancement, graph structure learning, and dual-branch time-frequency feature extraction, demonstrating optimal performance.

D. Comparative Experiments

To comprehensively validate the effectiveness and advantages of the proposed method, comparative experiments were conducted against the following four existing approaches:

(1) MTAD-GAT [26]: This model integrates a one-dimensional CNN, Graph Attention Mechanism (GAT), and Gated Recurrent Unit (GRU) to construct a multivariate time series anomaly detection framework that fuses reconstruction and prediction strategies. Specifically, it first extracts features from each dimension of the time series via 1D convolutions. Subsequently, two independent GAT modules model temporal correlations and feature dependencies in the sequence data. Finally, both the GAT-processed features and original inputs are fed into a GRU for reconstruction and future trend prediction.

(2) GAT-GRU [9]: This approach emphasizes extracting complex feature information from multiple dimensions (including temporal, modal, and spatial). The model first employs a graph attention mechanism to model each node across temporal and modal dimensions, extracting local and global dynamic features. Subsequently, a GRU captures long-term dependencies and performs dimensionality reduction on the data. GAT is then reapplied to extract spatial feature information, and the input data is reconstructed to identify anomalies based on reconstruction errors.

(3) GLSL [11]: This method transforms wireless sensor network (WSN) data into multiple graph structures from a modal perspective. GAT is applied to extract features from graph data across different modalities in both temporal and spatial dimensions. Building upon this, GRU models long-term dependencies. Finally, it integrates both reconstruction and prediction strategies for sequence anomaly detection, enhancing the model's adaptability and detection accuracy across different modalities.

TABLE II.
COMPARISON OF EXPERIMENTAL RESULTS

Method	Precision (%)	Rec(%)	F1(%)
MTAD-GAT	77.5	87.0	82.0
GAT-GRU	93.3	87.5	90.3
GLSL	94.5	87.0	90.6
ours	91.04	94.09	92.52

The experimental results are shown in Table II. Our method achieves optimal or near-optimal performance in terms of

precision, recall, and F1 score. Notably, it attains an F1 score of 92.52%, outperforming all other comparison methods and demonstrating outstanding capability in WSN anomaly detection tasks.

First, the MTAD-GAT method introduces a graph attention mechanism to model temporal and feature dimensions. Its adjacency matrix is either static or constructed a priori, lacking a data-driven graph structure learning mechanism. This results in weak adaptability of the graph modeling process to the true inter-node relationships.

Furthermore, GAT-GRU attempts multidimensional graph modeling through a complex multi-level GAT fusion strategy. However, its topology remains dependent on static rules without enhanced topological learning. While achieving an F1 score of 90.3% and accuracy of 93.3%, its recall rate (87.5%) is slightly insufficient, indicating potential omissions in identifying all anomalous points.

Finally, the GLSL method constructs graph structures from a modal perspective and combines reconstruction with prediction mechanisms to enhance detection robustness, achieving an F1 score of 90.6%, placing it among the more advanced existing approaches. However, its modal partitioning strategy is relatively fixed, failing to dynamically learn the coupling relationships and importance differences between the time and frequency domains, leaving room for optimization in the expressive power of anomaly fusion features.

Our proposed method significantly outperforms the aforementioned approaches in overall performance. Notably, it maintains a precision rate of 91.04% while achieving a recall rate as high as 94.09%, demonstrating not only accurate anomaly identification but also strong anomaly coverage capabilities.

To further validate the anomaly detection performance of the proposed TE-MSTAD network model across diverse application scenarios, this paper designed comparative experiments based on indoor and outdoor multi-scenario environments. The typical indoor sensor network dataset IBRL and the self-built outdoor LoRA-OSD real-world monitoring dataset were selected, covering complex data features from multi-modal, multi-node collection in wireless sensor networks under varying conditions. By training and testing the model on both datasets, we comprehensively evaluate the proposed method's generalization capability and robustness across multiple scenarios and data distributions. Specific experimental results are shown in Table III.

TABLE III.

EXPERIMENTAL RESULTS ACROSS DIFFERENT SCENARIOS

Dataset	Precision (%)	Rec(%)	F1(%)
IBRL	91.04	94.09	92.52
LoRA-OSD	92.57	94.05	93.28

The table demonstrates that the proposed TE-MSTAD model achieves outstanding anomaly detection performance on both datasets, maintaining high levels across all metrics. For the indoor IBRL dataset, the model exhibits high recall in capturing complex multi-node, multi-modal relationships, indicating strong sensitivity to anomalous data. On the outdoor LoRA-OSD dataset with complex scenarios, the model demonstrates

robust adaptability and stability, achieving an F1 score slightly higher than IBRL. This validates TE-MSTAD's generalization capability and robustness across diverse environments. This further demonstrates that TE-MSTAD can effectively enhance the accuracy and robustness of anomaly detection in wireless sensor networks, exhibiting strong practical potential in complex, multi-modal, multi-node industrial scenarios.

E. Visualization Analysis

This section presents a case study analyzing the anomaly detection performance of the proposed model using selected experimental samples. Fig. 4 displays temperature and humidity data collected from Node 18 over 3,400 time steps, with correlation anomalies intentionally introduced. The red and green lines represent the sensor's temperature and humidity data, respectively. The black line indicates the true anomaly label, the blue line shows the model's prediction results, and the orange annotations mark misclassified points. This visualization clearly demonstrates the model's effectiveness in handling multimodal correlation anomalies, further validating the collaborative role and rationality of each submodule in detecting correlation anomalies. Fig. 5(a) displays the temperature data sequence collected at node 18 over 1296 time points from the IBRL dataset. The blue line represents the original normal data, while red, green, and purple correspond to injected point anomalies, context anomalies, and collective anomalies, respectively. In Fig. 5(b), test samples were constructed using a sliding window method (window size set to 200), and anomaly detection was performed based on the model's predictions. The upper section of Fig. 5(b) shows the label distribution for different anomaly types, while the lower section displays the detection result labels. The comparison reveals that the model predictions align highly with the true labels in the vast majority of cases. The few misclassifications primarily occur when the sliding window first covers an anomaly point or in segments with intense fluctuations in the original data. Overall, the detection method developed in this study accurately identifies multiple types of anomalous data, demonstrating strong practicality and robustness. Fig. 6(a) displays the temperature time-series data for three adjacent nodes (23, 25, 27), with a point anomaly added at node 23. Fig. 6(b) presents the corresponding anomaly detection results for these nodes. The figures reveal that the model successfully identified all point anomalies at node 23, demonstrating strong detection capability for handling localized temporal disturbances. Simultaneously, no false positives occurred at nodes 25 and 27, indicating that explicit modeling of graph structural dependencies enables the model to effectively confine the impact of anomalous responses. This confines anomalies primarily to the disturbed node, thereby preventing generalized false detections caused by the propagation of spatial correlation information.

> REPLACE THIS LINE WITH YOUR MANUSCRIPT ID NUMBER (DOUBLE-CLICK HERE TO EDIT) <

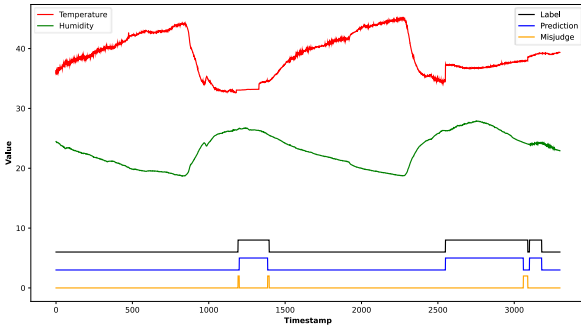
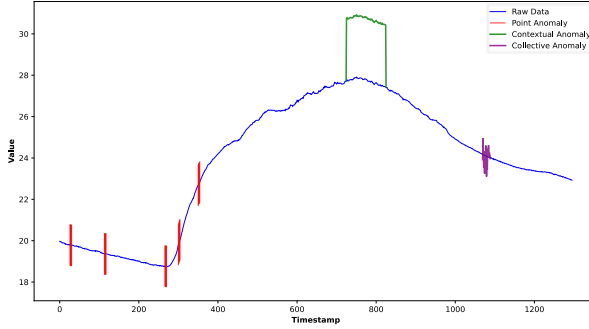
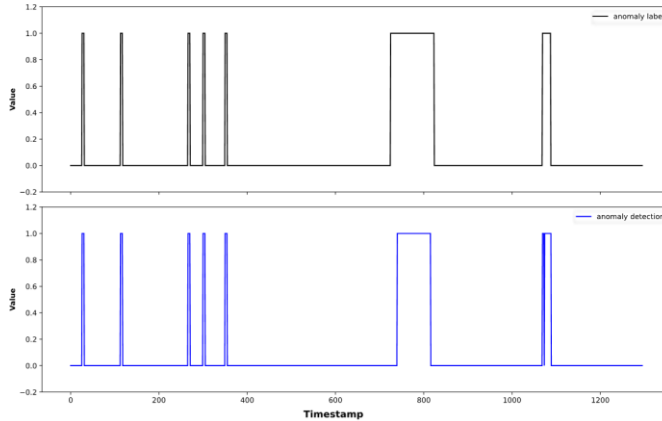


Fig. 4. Anomaly detection of multimodal correlations in WSN.

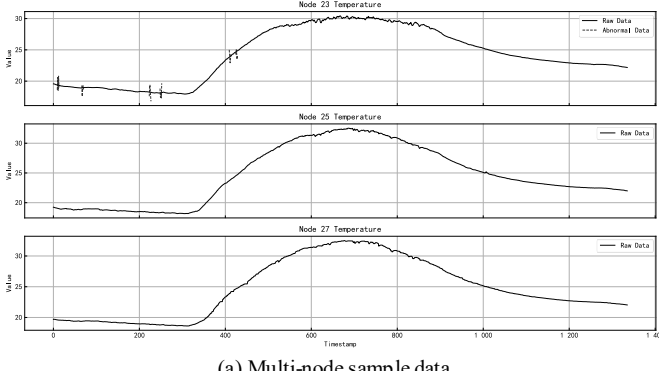


(a) Test sample data.



(b) Sample labels and anomaly detection labels.

Fig. 5. WSN single-node anomaly detection.



(a) Multi-node sample data.

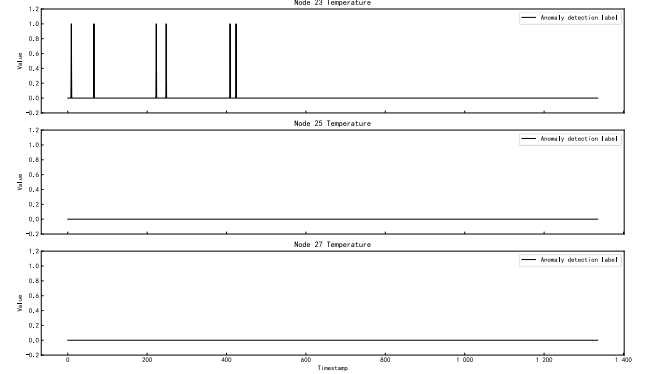


Fig. 6. Correlation anomaly detection among multiple nodes in WSN.

VI. CONCLUSION

This paper proposes a multi-modal spatio-temporal anomaly detection method that enhances topo-logical information by integrating temporal and frequency domain features. Building upon an improved RWKV model, the method introduces cross-extraction blocks and employs a dual-branch network architecture. This approach fully exploits spatio-temporal dependencies among multi-node multi-modal data, significantly enhancing anomaly detection performance. Furthermore, leveraging information enhancement principles, the method integrates graph neural network submodels and jointly learns graph structure adjacency matrices across time and frequency domains, thereby strengthening its ability to capture spatial correlations among different nodes. Experimental results demonstrate superior performance of the proposed method compared to traditional multi-time-series detection models on public datasets. Furthermore, experiments applying the model to both public and real-world datasets achieve excellent detection outcomes, validating its robust detection capability and generalization performance. Future research may further explore lightweight architectures, spatio-temporal adaptive mechanisms, and diverse training strategies to enhance the model's detection performance, deployability, and real-time capability in complex scenarios such as industrial IoT.

REFERENCES

- [1] T. M. Behera and S. K. Mohapatra, "A novel scheme for mitigation of energy hole problem in wireless sensor network for military application," *Int. J. Commun. Syst.*, vol. 34, no. 11, p. 4886, 2021.
- [2] T. -B. Dang, D.-T. Le, T.-D. Nguyen, M. Kim, and H. Choo, "Monotone split and conquer for anomaly detection in IoT sensory data," *IEEE Internet of Things Journal*, vol. 8, no. 20, pp. 15468–15485, 2021.
- [3] M. E. Haque, M. Asikuzzaman, I. U. Khan, I.-H. Ra, M. S. Hossain, and S. B. H. Shah, "Comparative study of IoT-based topology maintenance protocol in a wireless sensor network for structural health monitoring," *Remote Sensing*, vol. 12, no. 15, p. 2358, 2020.
- [4] A. J. Wilson and A. S. Radhamani, "Real-time flood disaster monitoring based on energy-efficient ensemble clustering mechanism in wireless sensor network," *Softw. Pract. Exp.*, vol. 52, no. 1, pp. 254–276, 2022.
- [5] T. Ali, M. Irfan, A. Shaf, A. S. Alwadie, A. Sajid, M. Awais, and M. Aamir, "A secure communication in IoT-enabled underwater and wireless sensor network for smart cities," *Sensors*, vol. 20, no. 15, p. 4309, 2020.
- [6] D. E. Boubiche, S. Athmani, S. Boubiche, A. S. Rajawat, S. B. Goyal, and A. A. Hussein, "Cybersecurity issues in wireless sensor networks: Current challenges and solutions," *Wireless Personal Communications*, vol. 117, no. 1, pp. 177–213, 2021.
- [7] H. N. Zhang, S. P. Xing, and J. N. Wang, "Security and application of wireless sensor network," *Procedia Comput. Sci.*, vol. 183, pp. 486–492, 2021.

> REPLACE THIS LINE WITH YOUR MANUSCRIPT ID NUMBER (DOUBLE-CLICK HERE TO EDIT) <

[8] L. Ma, N. Li, Y. Guo, M. Huang, S. Yang, X. Wang, and H. Zhang, "Learning to optimize: Reference vector reinforcement learning adaption to constrained many-objective optimization of industrial copper burdening system," *IEEE Trans. Cybern.*, vol. 52, no. 12, pp. 12698–12711, 2022.

[9] Q. Zhang, M. Ye, and X. Deng, "A novel anomaly detection method for multimodal WSN data flow via a dynamic graph neural network," *Connect. Sci.*, vol. 34, no. 1, pp. 1609–1637, 2022.

[10] X. Huang, F. Zhang, H. Fan, and L. Xi, "Multimodal adversarial learning based unsupervised time series anomaly detection," *Journal of Computer Research and Development*, vol. 58, no. 8, pp. 1655–1667, 2021.

[11] M. Ye, Q. Zhang, X. Xue, Y. Wang, Q. Jiang, and H. Qiu, "A novel self-supervised learning-based anomalous node detection method based on an autoencoder for wireless sensor networks," *IEEE Systems Journal*, 2024.

[12] R. Ahmad and E. H. Alkhammash, "Online adaptive Kalman filtering for real-time anomaly detection in wireless sensor networks," *Sensors*, vol. 24, no. 15, p. 5046, 2024, doi: 10.3390/s24155046.

[13] L. Ma, Y. Qian, G. Yu, Z. Li, L. Wang, Q. Li, X. Wang, and G. Han, "TBCIM: Two-level blockchain-aided edge resource allocation mechanism for federated learning service market," *IEEE/ACM Trans. Netw.*, 2025, doi:10.1109/TON.2025.3589017.

[14] N. Li, B. Xue, L. Ma, and M. Zhang, "Automatic fuzzy architecture design for defect detection via classifier-assisted multiobjective optimization approach," *IEEE Trans. Evol. Comput.*, 2025, doi:10.1109/TEVC.2025.3530416.

[15] M. Ye, Z. Jiang, X. Xue, X. Li, P. Wen, and Y. Wang, "A novel spatiotemporal correlation anomaly detection method based on time-frequency-domain feature fusion and a dynamic graph neural network in wireless sensor network," *IEEE Sens. J.*, vol. 25, no. 9, pp. 15548–15563, May 2025, doi: 10.1109/JSEN.2025.3549220.

[16] M. Dener, C. Okur, S. Al, and A. Orman, "WSN-BFSF: A new data set for attacks detection in wireless sensor networks," *IEEE Internet Things J.*, vol. 11, no. 2, pp. 2109–2125, Jan. 2024, doi: 10.1109/JIOT.2023.3292209.

[17] A. Javed, H. Larijani, A. Ahmadiania, R. Emmanuel, M. Mannion, and D. Gibson, "Design and implementation of a cloud-enabled random neural network-based decentralized smart controller with intelligent sensor nodes for HVAC," *IEEE Internet Things J.*, vol. 4, no. 2, pp. 393–403, Apr. 2017, doi: 10.1109/JIOT.2016.2627403.

[18] S. Felici-Castell, J. Segura-Garcia, J. J. Perez-Solano, R. Fayos-Jordan, A. Soriano-Asensi, and J. M. Alcaraz-Calero, "AI-IoT low-cost pollution-monitoring sensor network to assist citizens with respiratory problems," *Sensors*, vol. 23, no. 23, p. 9585, 2023, doi: 10.3390/s23239585.

[19] W. Jiang, J. Wang, K.-L. Hsiung, and H.-Y. Chen, "GRNN-based detection of eavesdropping attacks in SWIPT-enabled smart grid wireless sensor networks," *IEEE Internet Things J.*, vol. 11, no. 22, pp. 37381–37393, Nov. 2024, doi: 10.1109/JIOT.2024.3443277.

[20] A. Vaswani, N. Shazeer, N. Parmar, J. Uszkoreit, L. Jones, A. N. Gomez, L. Kaiser, and I. Polosukhin, "Attention is all you need," *Proc. 31st Conf. Neural Information Processing Systems (NIPS 2017)*, Curran Associates, Inc., Red Hook, NY, USA, Dec. 2017, pp. 5998–6008.

[21] S. Xie, Y. Li, Y. Ma, and Y. Wu, "AutoGMM-RWKV: A detecting scheme based on attention mechanisms against selective forwarding attacks in wireless sensor networks," *IEEE Internet Things J.*, vol. 12, no. 4, pp. 4403–4419, Feb. 2025, doi: 10.1109/JIOT.2024.3484999.

[22] K. Gröchenig, "Uncertainty principles for time-frequency representations," *Adv. Gabor Anal.*, pp. 11–30, 2003.

[23] J. Liu, Y. Sha, W. Zhang, Y. Yan, and X. Liu, "Anomaly detection method for industrial control system operation data based on time-frequency fusion feature attention encoding," *Sensors*, vol. 24, no. 18, p. 6131, 2024, doi: 10.3390/s24186131.

[24] T. K. K. Ho, A. Karami, and N. Armanfard, "Graph-based time-series anomaly detection: A survey and outlook," *arXiv preprint arXiv:2302.00058*, 2024.

[25] M. Zhang, J. Guo, X. Li, and R. Jin, "Data-driven anomaly detection approach for time-series streaming data," *Sensors*, vol. 20, no. 19, p. 5646, 2020, doi:10.3390/s20195646.

[26] T. Zhao, T. Jiang, N. Shah, and M. Jiang, "A synergistic approach for graph anomaly detection with pattern mining and feature learning," *IEEE Transactions on Neural Networks and Learning Systems*, vol. 33, no. 6, pp. 2393–2405, June 2022, doi:10.1109/TNNLS.2021.3102609.

[27] M. Zhao, H. Peng, L. Li, and Y. Ren, "Graph attention network and Informer for multivariate time series anomaly detection," *Sensors*, vol. 24, no. 5, p. 1522, 2024, doi:10.3390/s24051522.

[28] H. Zhao and H. Nambo, "Plant biopotential sensing based on generative adversarial networks for environmental anomaly detection," *IEEE Sensors Journal*, vol. 23, no. 23, pp. 29793–29803, Dec. 2023, doi:10.1109/JSEN.2023.3323147.

[29] Y. Li, Y. Sun, X. Chen, Q. He, X. Long, Z. Peng, and L. Yang, "Adversarial regularized graph autoencoder for intelligent anomaly detection with multisensor signal fusion," *IEEE Transactions on Instrumentation and Measurement*, vol. 74, Art. no. 3534011, pp. 1–11, 2025, doi:10.1109/TIM.2025.3565242.

[30] R. Doroudi, S. H. Lavassani, and M. Shahrouzi, "Optimal tuning of three deep learning methods with signal processing and anomaly detection for multi-class damage detection of a large-scale bridge," *Structural Health Monitoring*, vol. 23, no. 5, pp. 3227–3252, 2024, doi:10.1177/14759217231216694.

[31] L. Ma, Y. Zhou, Y. Ma, G. Yu, Q. Li, and Q. He, "Defying multi-model forgetting in one-shot neural architecture search using orthogonal gradient learning," *IEEE Trans. Comput.*, vol. 74, no. 5, pp. 1678–1689, 2025, doi:10.1109/TC.2025.3540650.